as well as ferric chelators should be considered in iron chelation therapy. A23187 has a number of the structural features required for rapid membrane transport of iron and had potential application in mixed ligand chelation therapy. However, this study has shown the structures of the Fe^{2+} and Ca^{2+} complexes to be closely similar. Hence, attempts to design a ligand analogue of A23187 with enhanced specificity for iron seem unlikely to be successful.

Acknowledgments. The A23187 was generously donated by Dr. Robert L. Hamill of the Lilly Research Laboratories, Indianapolis, IN. We are grateful to Dr. J. M. Harrowfield for helpful discussions and assistance. The investigation was supported by funds from the Australian Research Grants Committee, the National Health and Medical Research Council (No. 81/3285), and the Telethon Foundation.

Registry No. $Fe(A23187)_2 \cdot 2C_2H_5OH$, 89346-13-4.

Supplementary Material Available: Listings of measured structure amplitudes, calculated structure factors, and anisotropic thermal parameters of the iron atom are available (13 pages). Ordering information is given on any current masthead page.

Amorphous Chain Complexes $MM'(EDTA)(H_2O)_4 \cdot 2H_2O$. LAXS Investigation of the Local Structure and Magnetic Behavior

Alain Mosset, Jean Galy,* Eugenio Coronado,† Marc Drillon,† and Daniel Beltran‡

Contribution from the Laboratoire de Chimie de Coordination du CNRS, 31400 Toulouse, France, ENSCS, Dêpartement Sciences des Matêrianx, 67008 Strasbourg, France, and Departamento de Quimica Inorganica, Universidad de Valencia, Valencia, Spain.
Received October 4, 1983

Abstract: The amorphous $MM'(EDTA)(H_2O)_4 \cdot 2H_2O$ (MM' = NiCo, NiNi) materials comprise infinite chains built up with alternated "hydrated" and "chelated" octahedra bridged by carboxylate groups: ...–$M'(H_2O)_4$–M(EDTA)–$M'(H_2O)_4$–.... Investigation by the LAXS method allows one to precise the following points: (i) the coordination of the EDTA ligand is strictly the same as in the crystalline phase, i.e., hexacoordination toward the M atom and two bridging groups; (ii) the refinement of the MM'M angle of the zigzag infinite chain has been carried out with a precision of 5°; (iii) it was further possible to obtain a partial refinement of the bridging group geometry. The magnetic behavior is discussed in terms of infinite chains of conventional spin assuming a J parameter distribution and a Lande-factor alternation. The results, showing the essential role of the superexchange angle on J values, are in good agreement with structural data.

Extensive studies in the field of polymeric transition-metal complexes have provided valuable information on the correlations between structure and magnetic properties.[1] Thus, in a one-dimensional system with one kind of antiferromagnetically exchange-coupled ions, the temperature dependence of the maximum susceptibility is shown to be related to the strength of the interaction.[2] Such systems have been extensively studied both from the experimental and the theoretical point of view, whatever the dimensionality of this interaction.[3-5]

In contrast, random exchange chains exhibiting some degree of structural disorder have mainly been investigated for their transport properties. The materials reported so far are highly conducting organic charge-transfer salts generally based on the TCNQ molecule as acceptor.[6-11]

A disordered system may be described from structural features even if it is induced by physical phenomena. Two models are currently involved when describing disordered chains: one refers to distinct-sized finite fragments randomly arranged more or less cross-linked, and the other refers to a random distribution of the bond lengths and bond angles between the connected ions. The first case arises when defects are chemically or physically induced, for example, by the introduction of nonmagnetic impurities or by irradiation; the second is better adapted when dealing with flexible chains such as ribbons where interactions only occur within a given ribbon. Obviously, owing to the different frameworks, both arrangements are expected to show well-distinct behaviors from a magnetic point of view.[12]

In this paper, investigation of the correlation of local order and magnetic properties in two amorphous complexes, $Ni_2(EDTA) \cdot 6H_2O$ and $NiCo(EDTA) \cdot 6H_2O$, is carried out. Both complexes belong to a series formulated as $MM'(EDTA) \cdot 6H_2O$ (M and M' are divalent first-row metals). They have been isolated, by appropriate synthesis methods, as crystalline and amorphous varieties.

The magnetic behavior of the crystallized complexes has been previously discussed in terms of well-isolated exchange-coupled chains, in agreement with the structure.[13] It has been specifically emphasized that, for distinct M and M' sublattices, spin alternation results in a ferromagnetic one-dimensional behavior.[14,15]

* Laboratoire de Chimie de Coordination du CNRS.
† ENSCS, Dêpartement Sciences des Matêrianx.
‡ Departamento de Quimica Inorganica, Universidad de Valencia.

(1) Ginsberg, A. P. *Inorg. Chim. Acta Rev.* **1971**, *5*, 45. Sinn, E. *Coord. Chem. Rev.* **1970**, *5*, 313.
(2) Bonner, J. C.; Fisher, M. E. *Phys. Rev. A* **1964**, *A135*, 640.
(3) Weng, C. Y. Ph.D. Thesis, Carnegie Institute of Technology, 1968.
(4) Blote, H. W. J. *Physica B* **1975**, *79B*, 427-435.
(5) De Jongh, L. J.; Miedema, A. R. *Adv. Phys.* **1974**, *23*, 1-9.
(6) Bulaevskii, L. N.; Zvarykina, A. V.; Karimov, Yu. S.; Lyobovskii, R. B.; Shchebolev *Zh. Eksp. Teor. Fiz.* **1962**, *62*, 725 (*Sov. Phys. JETP* (*Engl. Trans.*) **1972**, *35*, 384).
(7) Azevedo, L. J.; Clark, W. B. *Phys. Rev. B* **1977**, *B16*, 3252-3255.
(8) Delha's, P.; Keryer, G.; Flandrois, S.; Manceau, J. P. *Phys. Status Solidi B* **1977**, *B80*, 125-129.
(9) Bozler, H. M.; Gould, C. M.; Bartolac, T. J.; Clark, W. G.; Glover, K.; Sanny, J. *Bull. Am. Phys. Soc.* **1980**, *25*, 217.
(10) Miljak, M.; Korin, B.; Cooper, J. R.; Holzer, K.; Janossy, A. *J. Phys.* **1980**, *41*, 639-645.
(11) Valade, L.; Cassoux, P.; Gleizes, A.; Interrante, L. V. *J. Phys.*, in press.
(12) Scott, J. C.; Garito, A. F.; Heeger, A. J.; Nannelli, P.; Gillman, H. B. *Phys. Rev. B* **1976**, *B12*, 356-361.
(13) Beltran, D.; Escriva, E.; Drillon, M. *J. Chem. Soc., Faraday Trans. 2* **1982**, *78*, 1773-1779.

0002-7863/84/1506-2864$01.50/0

Table I. Elemental Analysis of [NiNi] and [NiCo] Complexes

	% C		% N		% H		% Ni		% Co	
complex	C	F	C	F	C	F	C	F	C	F
[NiNi]	23.39	22.30	5.46	5.21	4.71	4.63	22.87	20.88		
[NiCo]	23.38	21.90	5.45	5.44	4.71	4.50	11.43	11.16	11.47	10.40

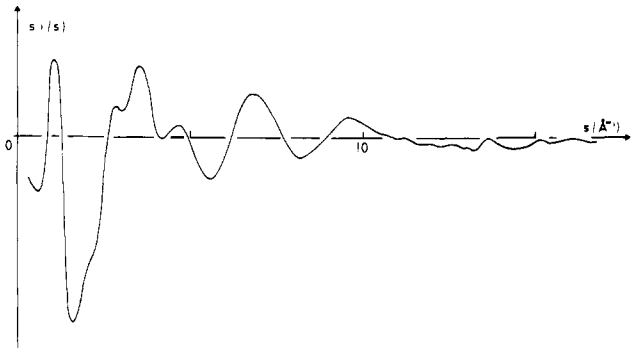

Figure 1. Experimental curve of $si(s)$ vs. s for $Ni_2(EDTA)(H_2O)_4 \cdot 2H_2O$.

A similar study on the amorphous complexes which primarily seems unrealistic is developed here in the light of structural investigations by large-angle X-ray scattering (LAXS) carried out in our laboratory both in its technical and applicational features.[16-19]

Experimental Section

Preparation of the Complexes. An aqueous solution of $(EDTA)Na_4$ was mixed with stoichiometric quantities of the corresponding nitrates of M and M′ (where M and M′ = Co(II) or Ni(II)) dissolved in a minimum quantity of water. After filtration of the resulting solution, excess acetone was added with stirring and a slimy solid was obtained. This solid, separated by decantation and dried in air, appears as blue ([NiNi] complex) or purple ([NiCo] complex) pellets. Elemental analysis data are reported in Table I.

Large-Angle X-ray Scattering (LAXS) Data Collection. (i) Samples. [NiCo] Complex: the sample was a 0.165-mm-thick violet thin platelet. **[NiNi] Complex**: the platelets of the sample obtained after slow evaporation were too small to allow valuable data collection. Consequently, the compound was carefully ground and pressed (3000 kg/cm^2) into a 0.33-mm-thick pellet.

(ii) Data Collection. The diffuse spectrum scattered by the sample irradiated with graphite-monochromatized molybdenum Kα radiation was obtained by using an automatic diffractometer. About 450 intensities corresponding to equidistant s points ($s = 4\pi(\sin\theta/\lambda)$, $\Delta s = 0.035363$) were collected (in the range $2° < \theta < 70°$) (2θ is the diffusion angle). The stability of the X-ray flux and of the sample was checked by frequent repetition of measurements at angles conveniently spread out in the θ range. All the measurements were carried out at 22 °C.

Scattered intensities were corrected for polarization and absorption effects (namely $I_c(s)$), then normalized by comparison, in the vicinity of high θ angles, with the sum of coherent and incoherent independent intensities. The normalization factor K derived from this data treatment is in good agreement with those determined from Norman's[20] and Krogh-Moe's[21] methods. Atomic scattering factors, $f_i(s)$ for all the atoms, were those proposed by Cromer and Waber;[22] Compton diffusion factors were taken from tables published by Cromer.[23]

Reduced intensities, $i(s)$, were calculated as follows:

$$i(s) = KI_c(s) - \sum_i n_i[(f_i(s) + \Delta f'_i)^2 + \Delta f''^2_i + I_{i(\text{inch})}(s)]$$

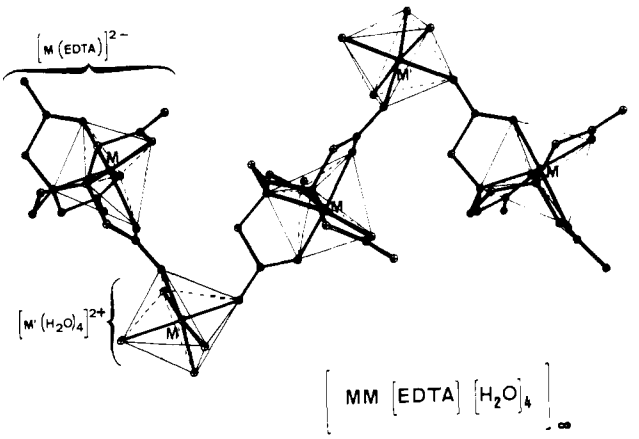

Figure 2. Geometry of the infinite zigzag strings $[MM'(EDTA)(H_2O)_4]_\infty$.

where K is the normalization constant, $I_c(s)$ is the corrected intensities, n_i is the number of atoms i in the chosen unit volume, $f_i(s)$ is the atomic scattering factor, $\Delta f'_i$ and $\Delta f''_i$ are the real and imaginary part of the anomalous dispersion, and $I_{i(\text{inch})}(s)$ is the total incoherent radiation for the atom i. The product $si(s)$ vs. s is represented in Figure 1 for the compound $Ni_2(EDTA)(H_2O)_4 \cdot 2H_2O$. The radial distribution $D(r)$ is then expressed under the form

$$D(r) = 4\pi r^2\rho_0 + 2r\pi^{-1}\int_{s_{\min}}^{s_{\max}} si(s)M(s)\sin(rs)\,ds$$

where ρ_0 is the average electronic density of the sample and $M(s)$ is a modification function defined by $f^2_{Ni}(0)/f^2_{Ni}(s)\exp(-s^2/100)$.

The corresponding theoretical intensities were calculated from the relation

$$i(s) = \sum_i\sum_j f_i(s)f_j(s)\frac{\sin(r_{ij}s)}{r_{ij}s}\exp(-b_{ij}s^2)$$

where r_{ij} is the interatomic distance between atoms i and j and b_{ij} a temperature factor affecting this interaction.

All calculations were performed by using an Apple II Plus microcomputer with our LASIP program written in Basic; the structure of this program is similar to the KURVLR program of Johansson and Sandström.[24]

Magnetic Measurements. The magnetic susceptibilities were performed in the range 2.3-100 K by using a pendulum-type apparatus equipped with a He cryostat. The uncertainty on the data is lower than 0.1 K for temperatures and 2×10^{-5} emu mol^{-1} for susceptibilities.

All magnetic measurements reported hereafter correspond to corrected values for the diamagnetic contribution estimated to be -170×10^{-6} emu mol^{-1} from Pascal's tables.

Structural Investigation

This structural investigation was meant to elaborate a possible structure for the amorphous variety of the complexes by confronting our results with those carried out[25] on the crystallized complex $Zn_2(EDTA)(H_2O)_4 \cdot 2H_2O$ and later confirmed[26] on an analogous compound, $Co_2(EDTA)(H_2O)_4 \cdot 2H_2O$. In fact, it proved that a whole family, namely $MM'(EDTA)(H_2O)_4 \cdot 2H_2O$, crystallizes with the same structure, as demonstrated by Beltran et al.[13] (M, M′ = Mg, Mn, Co, Ni, Cu, or Zn).

The structural organization consists of infinite zigzag strings of polymer-like compounds $[MM'(EDTA)(H_2O)_4]_\infty$ with alternate

(14) Drillon, M.; Gianduzzo, J. C.; Georges, R. *Phys. Lett. A* **1983**, *96A*, 413-416.
(15) Drillon, M.; Coronado, E.; Beltran, D.; Georges, R. *Chem. Phys.*, **1983**, *79*, 449.
(16) Galy, J.; Mosset, A.; Lecante, P. ANVAR French Patent 80.16170, 1980, and US Patent pending.
(17) Mosset, A.; Lecante, P.; Galy, J. *C. R. Hebd. Seances Acad. Sci., Ser. C* **1980**, *290C*, 325-328.
(18) Mosset, A.; Lecante, P.; Galy, J.; Livage, J. *Philos. Mag.* [*Part B*] **1982**, *46B*, 137-149.
(19) Galy, J.; Mosset, A. International Symposium: "Structure and Bonding in Noncrystalline Solids"; Reston, VA, July 23-26, 1983.
(20) Norman, N. *Acta Crystallogr.* **1957**, *10*, 370-373.
(21) Krogh-Moe, J. *Acta Crystallogr.* **1956**, *9*, 951-954.
(22) Cromer, D. T.; Waber, J. T. *Acta Crystallogr.* **1965**, *18*, 104.
(23) Cromer, D. T. *J. Chem. Phys.* **1969**, *50*, 4857-4860.
(24) Johansson, G.; Sandström, M. *Chem. Scr.* **1973**, *4*, 195-199.
(25) Pozhidaev, A. I.; Polynova, T. N.; Porai-Koshits, M. A.; Meronova, N. N. *Zh. Strukt. Khim.* **1973**, *14*, 570-571.
(26) McCandlish, L. F. K.; Michael, T. K.; Neal, J. A.; Lingafelter, E. C.; Rose, M. J. *Inorg. Chem.* **1978**, *6*, 1383-1394.

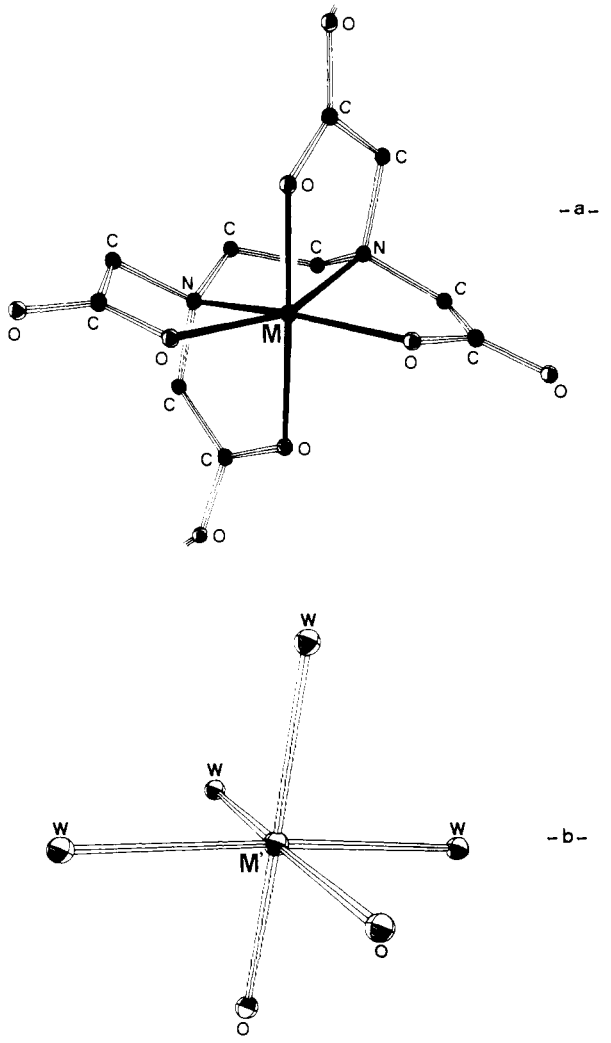

Figure 3. (a) Coordination scheme of the EDTA Ligand at the M site. (b) Geometry of the octahedral M′ site.

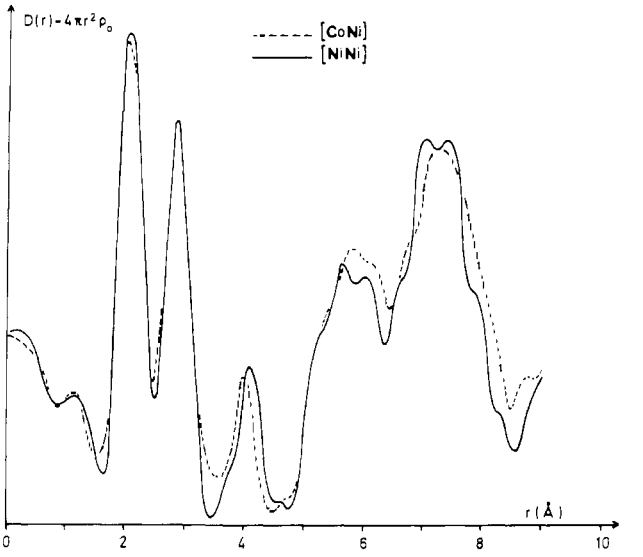

Figure 4. Comparison of the experimental radial distribution curves for [NiCo] (dotted line) and [NiNi] (full line) complexes.

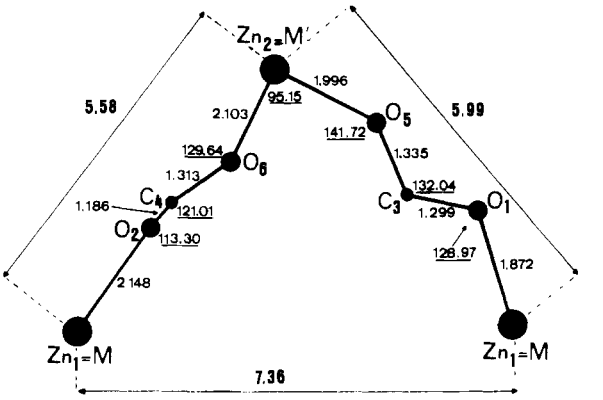

Figure 5. Details of the geometry of the zigzag strings in Zn_2-(EDTA)$(H_2O)_4$·$2H_2O$. The numbering scheme is the same as in ref 25.

metallic centers (Figure 2). One site (M) exhibits a hexacoordination through the ligand EDTA (Figure 3a), while the other (M′) is surrounded by two oxygen atoms in cis positions belonging to two bridging acid functions of the EDTA ligand and four water molecules (Figure 3b).

It clearly appears that the geometry of these chains is directly related to the dimensions of the triangle MM′M.

[NiCo] Complex. The local structure of this [MM′] family in its amorphous state was first performed on the complex NiCo(EDTA)$(H_2O)_4$·$2H_2O$.[27] The following results were brought out: (i) zigzag chains are present as in the crystalline state; (ii) the EDTA coordination scheme is identical; and (iii) some enlargment of experimental peaks in the experimental radial distribution function $[D(r) - 4\pi r^2\rho_0]_{expt}$ compared with the theoretical one $[D(r) - 4\pi r^2\rho_0]_{theor}$ can be fairly well explained by the coexistence in the amorphous state of chains showing the MM′M angle to vary slightly around a mean value of 79°.

[NiNi] Complex. The comparison between experimental radial distribution functions of both [NiCo] and [NiNi] amorphous compounds (Figure 4) leads to the following conclusions.

(i) These complexes have similar local structures: both exhibit curves characterized by nearly identical peaks roughly centered on the same r values.

(ii) A more accurate comparison shows that the [NiNi] curve exhibits a "slimming" and a partial resolution of the peaks centered at 5.8 and 7.2 Å, which could imply that the chain geometry distribution already mentioned for the [NiCo] complex is less broad and that extreme conformations coexist in the [NiNi] amorphous compound.

These preliminary observations drive us to elucidate the amorphous structure on the basis of two different chain geometries which both remain strongly related to the crystalline model.

Architecture of the Amorphous [NiNi] Complex: Refinement and Discussion. Figures 2 and 3 show that the hexacoordination of the EDTA ligand implies a quasi-locked conformation for this $(Ni^{II}(EDTA))^{2-}$ moiety. So, the variations of geometry are directly connected to the acid function bridges and to the chain angle MM′M.

Detailed interatomic distances for the crystalline [ZnZn] complex are reported in Figure 5. The "short" Zn_1–Zn_2 = 5.58 Å distance corresponds to a normal acid function O2–C4–O6, and the "long" one, Zn_2–Zn_1 = 5.99 Å, implies a rather distorted acid function O5–C3–O1. The third metal–metal distance, Zn_1–Zn_1 = 7.36 Å, is directly related to the angle O6–Zn_2–O5.

The experimental radial distribution function of the [NiNi] complex (Figure 4, full line) exhibits maxima centered around 5.8 and 7.2 Å which are resolved into peaks positioned at 5.67 and 6.02 Å, and 7.06 and 7.44 Å, respectively. Such maxima resulting from various contributions are mainly affected by the metal–metal distances even though metal–ligand and ligand–ligand interactions are able to affect the position of the metal–metal peaks.

A strong correlation then clearly appears between the interatomic distances issued from the radial distribution and the calculated distances, except the maximum at 7.06 Å which remains unexplained; a more sophisticated model was consequently developed. In order to elaborate this model, the angles O–Ni′–O,

(27) Mosset, A.; Coronado, E.; Galy, J. *C. R. Hebd. Seances Acad. Sci., Ser. B* **1983**, *296B*, 549–552.

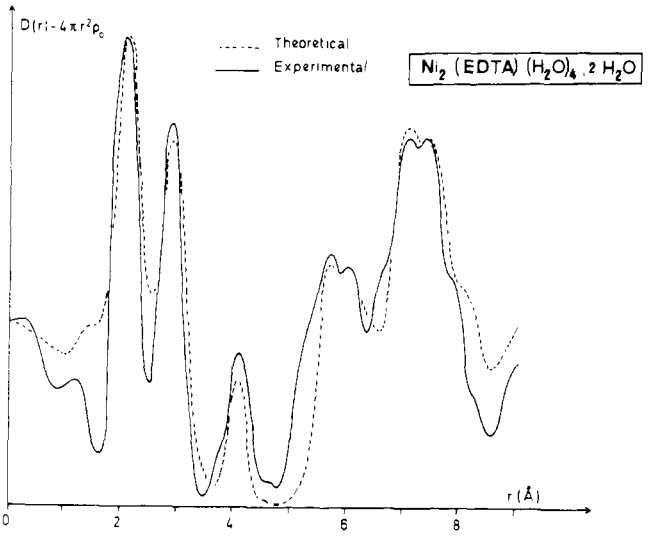

Figure 6. Comparison between the experimental (full line) and theoretical (dotted line) radial distribution curves for $Ni_2(EDTA)(H_2O)_4 \cdot 2H_2O$.

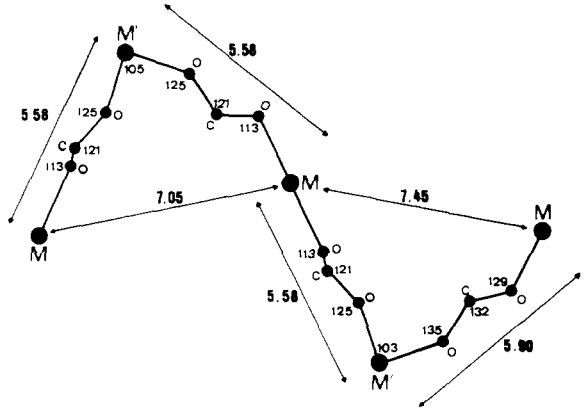

Figure 7. Schematic drawing of the proposed structural model.

Ni′–O–C, O–C–O, and C–O–Ni were allowed to vary, step by step, within the following limits: 110–145° for Ni′–O–C, O–C–O, and C–O–Ni and 85–110° for O–Ni′–O.

After each cycle of calculations, a theoretical radial distribution curve was calculated to determine specifically the influence of angle variations and to check the adequation between experimental and theoretical curves.

The final result is summarized in Figure 6; full and dotted lines represent the experimental curve of [NiNi] and the theoretical one for the selected model, respectively. This model is characterized by two triangular MM′M units with different geometries.

The first model is rather close to the crystal model with NiNi′ = 5.58 Å, Ni′Ni = 5.90 Å, and NiNi = 7.45 Å; it corresponds to dissymetric triangular units.

The second model is symmetrical, with NiNi′ = Ni′Ni = 5.58 Å and NiNi = 7.05 Å. Such a model is obtained by ascribing the values reported in Figure 7 to the variable parameters. Such a scheme calls for the following comments.

(i) The various geometries have been reported on the same drawing (Figure 7) for convenience. In fact, these geometries are probably randomly distributed within infinite chains.

(ii) These two extreme geometries imply the possibility of a distribution within the amorphous solid of units with intermediate interatomic distances and/or angles.

(iii) Bond angles are given as indications; the method utilized does not allow a better precision than 5° for each refined angle.

Theoretical calculations, based on several models with interatomic distances or angles different from those proposed, have shown strong discrepancies with the results experimentally established by LAXS studies. It is always of importance to notice the nonunivocal answer of such calculations when establishing a

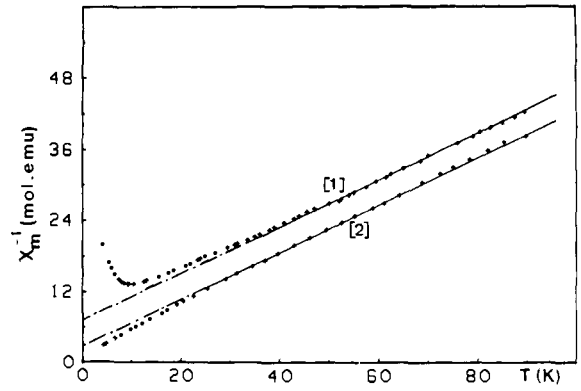

Figure 8. Magnetic behaviors of the crystallized **1** and amorphous **2** varieties of $Ni_2(EDTA)(H_2O)_4 \cdot 2H_2O$.

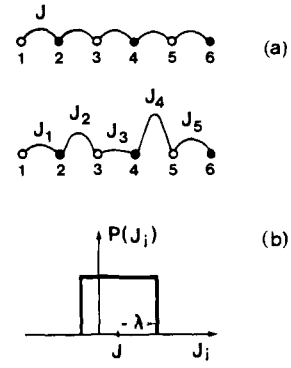

Figure 9. Schematic representation of infinite chains with a regular (a) or random exchange coupling (b); in the latter case, we have drawn the box-type distribution of the interactions.

structural model. Anyhow, the good agreement obtained after numerous calculations and the reasonable architectural model retained made us confident in the description of the amorphous complex $Ni_2EDTA(H_2O)_4 \cdot 2H_2O$ as infinite zigzag chains built up with octahedra ($Ni^{II}(EDTA)$) and ($Ni^{II}O_2(H_2O)_4$) sharing corners. Noncoordinated water molecules are randomly distributed in the sample.

Finally, such complexes should exhibit a peculiar magnetic behavior, the study of which is reported and discussed in the following section.

Discussion of the Magnetic Results

To begin with, let us compare the magnetic behaviors of the crystallized and amorphous varieties of $Ni_2(EDTA) \cdot 6H_2O$ through plots of the inverse susceptibility (χ_M^{-1}) vs. T (Figure 8).

We first note the sharp contrast existing at low temperatures since the inverse susceptibility of the amorphous phase tends to zero when cooling down to 0 K while it increases continuously in the crystallized state.

The minimum observed in the latter agrees with an antiferromagnetic exchange coupling between Ni(II) atoms located in zigzag chains; the exchange parameter determined in a previous study by means of an isotropic Heisenberg model was shown to be $J = -8.05$ cm^{-1}.[13] An extrapolation of the high-temperature behavior clearly indicates that the mean exchange interactions is weaker in the amorphous phase than in the ordered one.

Owing to the structural results, the amorphous state is first described by considering infinite "flexible" chains with a random exchange coupling between nearest neighbors (Figure 9).

As a second step, the role of defects giving rise to finite fragments is investigated.

Random Exchange Model. In order to take into account the distinction between the two unequivalent sites, even when occupied by the same atom, a linear system made of two alternating sublattices is considered.

The problem is solved in the classical spin approximation, which allows for the easy accounting of the J distribution.

Let the exchange Hamiltonian of an open linear chain be of the form:

$$\mathcal{H} = \sum_{i=1}^{N} H_i = -\sum_{i=1}^{N} J_i \vec{S}_i \vec{S}_{i+1}$$

The exchange parameter between S_i and S_{i+1}, defined as J_i, varies randomly along the chain.

Using the procedure described by Thorpe,[28] we show that the partition function,

$$Z = \int \frac{dS_1\, dS_2 \ldots dS_{N+1}}{(4\pi)^{N+1}} e^{\beta(H_1+H_2\ldots+H_N)}$$

may be evaluated by expanding the exponentials in terms of spherical harmonics $Y_1^m(S_i)$

$$e^{-\beta H_i} = 4\pi \sum_{l,m} \lambda_l(\beta J) Y_l^m(S_i) Y_l^{*m}(S_{i+1})$$

The $\lambda_l(\beta J)$ are related to Legendre polynomials $P_l(x)$, by means of

$$\lambda_l(\beta J) = \tfrac{1}{2} \int_{-1}^{+1} e^{\beta J x} P_l(x)\, dx$$

In the thermodynamic limit $N \to \infty$, the result expressed in closed form

$$Z = \prod_{i=1,N} \lambda_0(\beta J_i) = \prod_{i=1,N} \frac{\sinh(\beta J_i)}{\beta J_i}$$

only differs from that of a regular chain by the J distribution.[15]

The magnetic susceptibility is generally evaluated from the pair correlation functions $\langle \vec{S}_n \vec{S}_{n+p} \rangle$. In fact, in the case we are concerned with, we have to determine quantities such as $\langle \vec{M}_n \vec{M}_{n+p} \rangle = \langle g_n \vec{S}_n g_{n+p} \vec{S}_{n+p} \rangle$ with g_n depending on whether n is odd or even. We obtain

$$\langle \vec{M}_n \vec{M}_{n+p} \rangle = g_n g_{n+p} \prod_{i=n}^{n+p-1} F(\beta J_i)$$

with

$$F(\beta J_i) = \coth(\beta J_i) - 1/\beta J_i$$

Setting for convenience $g = \tfrac{1}{2}(g_1 + g_2)$ and $\delta g = \tfrac{1}{2}(g_1 - g_2)$ and considering the mean value $F_0 = \langle F(\beta J_i) \rangle$, obtaining the magnetic susceptibility is straightforward:

$$\chi_M = \frac{N\beta^2}{3kT}\left[g^2 \frac{1 + F_0}{1 - F_0} + \delta g^2 \frac{1 - F_0}{1 + F_0} \right]$$

Obviously, F_0 will depend on the kind of distribution chosen for the J parameter. It is generally assumed that J decreases exponentially with spin separation so that a distribution of the form $P(J_i) \simeq J_i^{-\alpha}$ should occur for small J values.[29]

In order to simplify the calculation, we have considered a square distribution centered at J and of width 2λ (Figure 9).

$$P(J_i) = 1/2\lambda \text{ for } -\lambda < J_i - J < \lambda$$

$$P(J_i) = 0 \text{ otherwise}$$

Such a distribution leads to the same kind of susceptibility divergence for $T \to 0$ K, as the previous one.[29] F_0 is then expressed under a condensed form as:

$$F_0 = \frac{kT}{2\lambda} \ln \frac{(J - \lambda)\sinh((J + \lambda)/kT)}{(J + \lambda)\sinh((J - \lambda)/kT)}$$

For discussing the influence of the relative width of the J_i distribution, we assumed $g_1 = g_2$, allowing for the first effect to be exactly defined (Figure 10).

When considering an antiferromagnetic coupling and for $\lambda = 0$, which corresponds to a regular chain with a single exchange parameter, the susceptibility shows a rounded maximum and a nonzero value at absolute zero, in agreement with Fisher's results.[30]

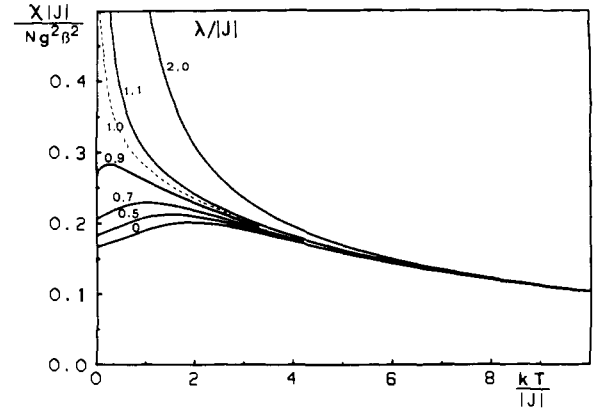

Figure 10. Reduced magnetic susceptibility of a classical spin randomly exchange-coupled chain. $\lambda/|J|$ is the ratio between the width of the distribution and the mean value of the interaction. All curves correspond to $J < 0$.

Table II. Least-Squares Refined Parameters for the Two Models

	J, cm^{-1}	λ, cm^{-1}	g_1/g_2	N	R
random exchange model					
[NiNi]	−2.40	7.15	2.03/2.25	∞	2.3×10^{-5}
[NiCo]	−5.95	13.40	4.76/2.10	∞	1.0×10^{-4}
finite fragment model					
[NiNi]	−1.82		2.10	20	2.2×10^{-3}

When $\lambda/|J|$ increases and as long as this ratio is below unity, we note a shift of the maximum toward low temperatures and a rise of the susceptibility in the $T = 0$ K limit. The curve corresponding to $\lambda = |J|$ is given on the graph with a dashed line; the low-temperature behavior is described by:

$$\frac{\chi|J|}{Ng^2\beta^2} = \frac{1}{12} \ln\left(\frac{4|J|}{kT}\right)$$

For upper values of $\lambda/|J|$, the divergence increases more quickly in agreement with the coexistence of finite fragments of ferromagnetic and antiferromagnetic interactions. So far as only the ferromagnetic couplings subsist, and for $\lambda = J$, at low enough temperatures, we obtain:

$$\frac{\chi|J|}{Ng^2\beta^2} = \frac{4}{3}\left(\frac{J}{kT}\right)^2 \frac{1}{\ln(4J/kT)}$$

Then, it may be emphasized that the divergence is less fast than in a regular ferromagnetic chain whose susceptibility varies as $(J/kT)^{-2}$. Obviously, such remarks which account for $g_1 = g_2$ fail as soon as a distinction between Lande factors is introduced. For instance, the antiferromagnetic chains, with $\lambda = 0$, will show the same limit behavior as the ferromagnetic one with one kind of magnetic site.[14]

Now, in order to compare theoretical prediction with experiment, we need the following scaling factors to account for real spins:

$$A \to A[S_1(S_1 + 1)S_2(S_2 + 1)]^{1/2} \text{ with } A = J \text{ or } \lambda$$

$$g_i \to g_i[S_i(S_i + 1)]^{1/2} \text{ with } i = 1,2$$

The ground configuration of the high-spin cobalt(II) being a Kramers doublet well-separated from the first excited configuration (200–300 cm^{-1}), the low-temperature behavior is described by $S = \tfrac{1}{2}$.[13] Further, a selective occupation of the two sites leading to a regular spin alternating chain as in the crystallized state is assumed for the [NiCo] complex.

(28) Thorpe, M. F. *J. Phys.* **1975**, *36*, 1177–1184.
(29) See: "Physics in One Dimension"; Bernasconi, J., Schneider, T., Eds.; Springer-Verlag: New York, 1981; p 294.
(30) Fisher, M. E. *Am. J. Physiol.* **1964**, *32*, 343–346.

For both complexes, the parameters obtained by a least-squares refinement are reported in Table II together with the sums of the squares of the relative deviations (R). The results, shown on Figure 11, call for the following remarks:

(i) The random exchange model describes very satisfactorily the experimental data in the studied temperature range. Only a small divergence is noticed below 2.5 K for $Ni_2(EDTA)\cdot 6H_2O$, which probably results from a zero-field splitting effect of the $^3A_2$ ground term.

(ii) The extrapolated nonzero value of χT observed in both cases when $T \rightarrow 0$ K appears to be well predicted from a distribution of the interactions including both ferromagnetic and antiferromagnetic couplings. Clearly, an infinite linear system with a distribution favoring only one kind of interaction would be irrelevant in the present case.

(iii) The width of the exchange distribution may seem overestimated. In fact, numerous studies have shown that small angular variations of metal-bridging ligand bonds may lead to drastic effects on the exchange magnitude. In order to check the independence of the parameters used in the fits, their values were determined in the crystallized $Ni_2(EDTA)\cdot 6H_2O$ complex, the structure of which corresponds to regular chains with a unique exchange constant.[13]

The parameters obtained, $J = -10.3$ K and $\lambda < 10^{-3}$ K, agree with the expected ones.

Finite Fragment Model. Owing to the temperature dependence of χT at low temperatures, it could be assumed that it results from noncompensated moments within finite chains of length N. In order to simplify the treatment, we have considered the same exchange constant along the fragments, namely J. This problem, solved by Fisher for classical spins with one kind of ion,[30] leads to the expression:

$$\chi = \frac{N_a \tilde{g}^2 \beta^2 S(S+1)}{3kT}\left[\frac{1+F}{1-F} - \frac{2F}{N}\frac{1-F^N}{(1-F)^2}\right]$$

with

$$F = \coth\frac{JS(S+1)}{kT} - \frac{kT}{JS(S+1)}$$

Following the same procedure as above, the data of the amorphous $Ni_2(EDTA)(H_2O)_4\cdot 2H_2O$ complex were fitted by means of the adjustable parameters N, g, and J. The results are reported in Table II and Figure 12.

Clearly, such an approach does not agree with experiment at low temperatures. If the $\tilde{g}$ value is close to the expected one for Ni(II), the average length of the fragments does not allow an explanation of the observed χT value as $T \rightarrow 0$ K ($\simeq 1.2$ emu). Thus, even if the presence of defects cannot be totally excluded, the hypothesis of quasi-infinite chains with a random distribution of the exchange couplings seems to be the more appropriate.

Conclusion

The goal of this study was to correlate the local structure of amorphous complexes $MM'(EDTA)(H_2O)_4\cdot 2H_2O$ with [MM'] = [NiNi] or [NiCo] to their magnetic behaviors. LAXS studies have clearly shown the great similitude between the structure of these complexes and the corresponding crystallized ones. We can only notice, as expected in the amorphous state, a distribution of bond angles between the connected ions so that the magnetic behavior cannot be merely described in terms of a regular Heisenberg chain. An analysis of the behavior by means of a classical treatment with a random distribution of the exchange interactions has been shown to be well adapted. In fact, it is worth noticing that the proposed approach calls for some approximations. The following may be especially pointed out:

(i) LAXS study investigations give an accurate picture of the structure up to about 9 Å; they do not allow the specification of the existence of defects, such as random ruptures of the chains.

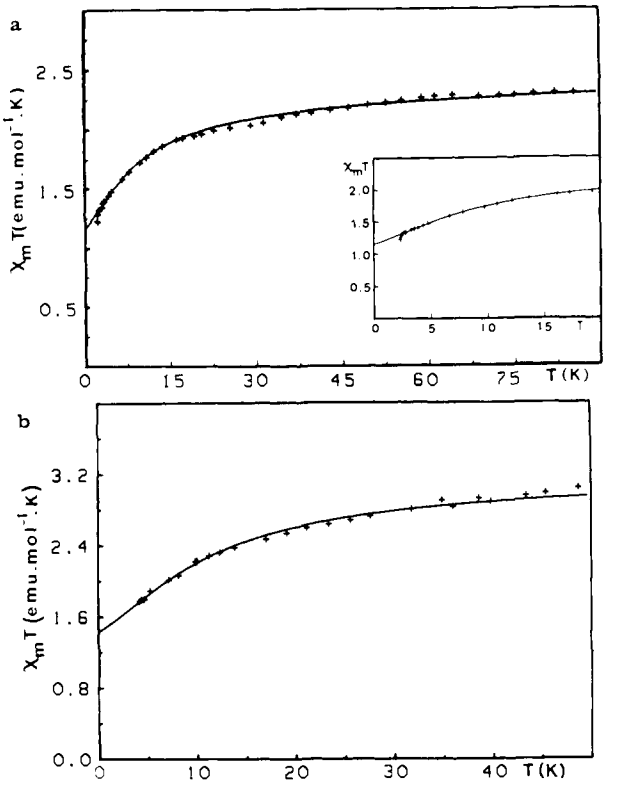

Figure 11. Comparison between experimental and theoretical (full line) magnetic behaviors for a square distribution of the next nearest neighbor interactions: (a) for the $Ni_2(EDTA)(H_2O)_4\cdot 2H_2O$ amorphous complex; (b) for the $NiCo(EDTA)(H_2O)_4\cdot 2H_2O$ amorphous complex. The values of the parameters are given in Table II.

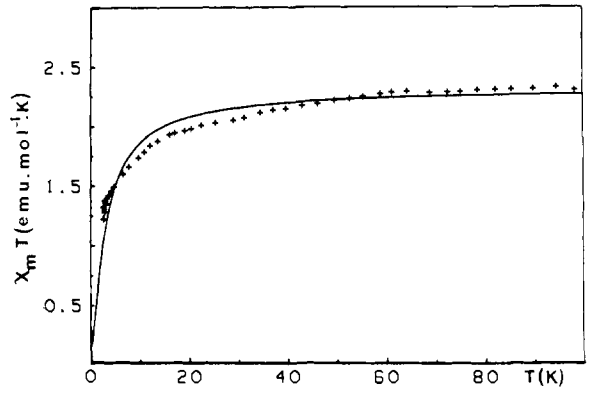

Figure 12. Experimental and theoretical (full line) behavior of $Ni_2(EDTA)(H_2O)_4\cdot 2H_2O$ from the finite fragment model. The values of the parameters are listed in Table II.

(ii) The use of a classical spin formalism, instead of a quantum one, is convenient in the present case, but gives an exchange constant determined by fitting which is overestimated by some 20%.

(iii) A square distribution of the exchange interactions does not correspond to a physical reality. In fact we show that more sophisticated $P(J_i)$ distribution lead to the same divergence of susceptibility as $T \rightarrow 0$ K.[29]

Finally, in spite of these remarks, the structural model defined by LAXS study appears as strongly supported by magnetic measurements thus showing the very good interplay between these complementary techniques when investigating these "magnetic amorphous materials".

Registry No. $Ni_2(EDTA)(H_2O)_4$, 89346-14-5; $NiCo(EDTA)(H_2O)_4$, 89395-88-0.